Eur. Phys. J. A (2023) 59:204
https://doi.org/10.1140/epja/s10050-023-01037-0

THE EUROPEAN PHYSICAL JOURNAL A

Review

Precise mass measurements of radioactive nuclides for astrophysics

Jason Clark[1,a], **Guy Savard**[1,b], **Matthew Mumpower**[2,3,c], **Anu Kankainen**[4,d]

[1] Physics Division, Argonne National Laboratory, Lemont, IL 60439, USA
[2] Theoretical Division, Los Alamos National Laboratory, Los Alamos, NM 87545, USA
[3] Center for Theoretical Astrophysics, Los Alamos National Laboratory, Los Alamos, NM 87545, USA
[4] Department of Physics, Accelerator Laboratory, University of Jyväskylä, 40014 Jyväskylä, Finland

Received: 10 March 2023 / Accepted: 16 May 2023
© UChicago Argonne, LLC, Operator of Argonne National Laboratory under exclusive licence to Società Italiana di Fisica and Springer-Verlag GmbH Germany, part of Springer Nature 2023
Communicated by Nicolas Alamanos

Abstract Much of astrophysics is fueled by nuclear physics with observables, such as energy output and elements produced, that are heavily dependent on the masses of the nuclides. A mass precision of at least 50 keV/c^2 for many rare nuclides is needed to adequately discriminate models that explain the observables. In recent decades, the development of new facilities and mass-measurement techniques has made available a wealth of precise and accurate mass data. The new data, in combination with novel codes and models, has greatly enhanced the understanding of astrophysical processes in the universe, but much is still to be learned.

1 Introduction

Stars have been responsible for the creation of the heaviest elements in nature, throughout their life time or in their deaths. As first described in the famous B^2FH paper [1], a number of astrophysical processes have been introduced to account for various features in the solar abundances. These astrophysical processes are driven by the nuclear fuel within stars and produce various observed phenomena.

This paper summarizes the recent progress made in our understanding of astrophysical processes with focus on the impact of precise mass measurements of the nuclides involved. A description of some select astrophysical processes is presented, followed by a review of the recent development and advances in facilities and mass measurement techniques. Present breakthroughs in the field are highlighted with the consideration of several impactful mass measurements.

2 Astrophysical processes

Of the astrophysical processes, there are two which have benefited most from recent precise mass measurements of the relevant nuclides: the *rp* process involving neutron-deficient nuclei, and the *r* process that involves neutron-rich nuclei. These processes and their dependence on nuclide masses are described in what follows.

2.1 *rp* process

The rapid proton capture (*rp*) process [2,3] takes place in hydrogen-rich conditions at temperatures above $T > 10^8$ K. In such conditions, it becomes possible to break out from the CNO cycles and proceed toward heavier elements via rapid proton captures. Here we focus on the *rp* process in type I x-ray bursts [4,5], which are binary star systems consisting of a neutron star and a main-sequence or red giant star that transfers hydrogen-rich material onto the surface of the neutron star. We note that rapid proton captures also play a role in novae and in the *νp* process [6,7], which takes place in neutrino-driven winds of core-collapse supernovae. The role of nuclear masses in these processes is analogous to what is described below for the *rp* process in type I x-ray bursts.

Type I x-ray bursts are powered by the *rp* process, which is initiated when sufficiently high temperatures and densities are reached in the hydrogen-rich layer accreted from the companion star onto the surface of the neutron star. The process starts with the triple-alpha process and CNO cycles,

[a] e-mail: jclark@anl.gov (corresponding author)
[b] e-mail: savard@anl.gov
[c] e-mail: matthew@mumpower.net
[d] e-mail: anu.kankainen@jyu.fi

Published online: 11 September 2023

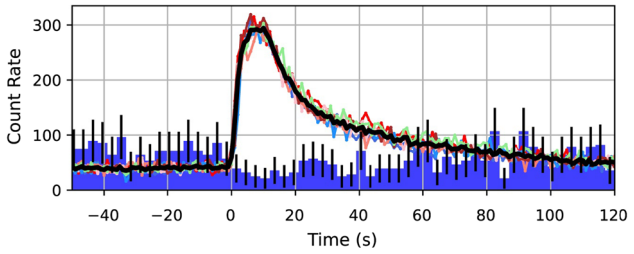

Fig. 1 Lightcurves for some of the x-ray bursts observed from 4U 1636–536 by NuSTAR in the 5–30 keV (colorful solid lines) and 30–79 keV (blue histograms) bands. The solid black curve shows the average light curve for the 5–30 keV band for which the time bin size is 1 s. The number of photons in the 30–79 keV band has been multiplied by 50 and the time bin is 4 s. Adopted and modified from Ref. [8] under CC BY 4.0

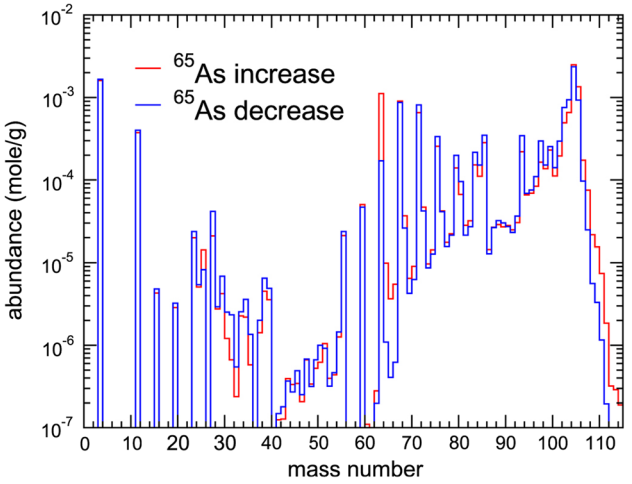

Fig. 2 The impact of the 85 keV uncertainty in the mass excess of ^{65}As from the 2012 Atomic Mass Evaluation [16] on the burst ashes for a type I x-ray burst model with very hydrogen-rich conditions that enable the rp process to extend beyond ^{64}Ge. This figure has been adopted from Ref. [14]

which heat the layer further and enable a pathway for (α, p) reactions in the lighter region, and eventually for the rp process. The thermonuclear runaway in the rp process proceeds along neutron-deficient radioactive nuclei up to $A \approx 110$ and swiftly generates a lot of energy observable in the x-ray region. When the process runs out of fuel, the produced radioactive nuclei decay back to stability releasing energy observed as a tail in the x-ray burst light curve. Examples of lightcurves observed from 4U 1636–536 are shown in Fig. 1.

Type-I x-ray burst lightcurves have typical rise times of around 1–10 s and their tail lasts from tens of seconds to minutes. The recurrence times vary considerably, from an hour to several hours. The information on type I x-ray light curves is increasing, with around 48 accreting neutron stars reported by the Rossi X-ray Timing Explorer [9] and around 7000 bursts listed in the Multi-INstrument Burst ARchive (MINBAR) [10]. Recently, results from the Neutron Star Interior and Composition Explorer (NICER) observations on type I x-ray bursts have also become available, see e.g. Refs. [8,11]. The released data sets provide new possibilities to explore these phenomena and require more accurate nuclear input to model the light curves. Sensitivity studies performed for the rp process calculations [12] have shown that the uncertainties in specific nuclear reaction rates introduce large variations in the calculated type I x-ray burst light curves. Even more importantly, nuclear masses, which are key inputs for the rp-process calculations as discussed below, can affect the calculated light curves significantly [5,13,14].

The rp process proceeds via proton captures until they become energetically unfavorable (low or negative proton-capture Q value). At such points, known as waiting points, the process has to wait for the much slower β^+ decay to happen. This results in accumulation of material in waiting points which, in turn, affects the final abundances of the process. The proton-capture Q value is directly determined using nuclear masses and for a nucleus (Z, N, A) it is the same as the proton separation energy of its isotone with $Z + 1$ protons, $Q_{p,\gamma}(Z, N, A) = S_p(Z + 1, N, A + 1)$.

In high-temperature environments the inverse photo-disintegration reactions (γ, p) also play a role and have to be taken into account in the calculations. According to the detailed balance principle, the photo-disintegration rate $\lambda_{\gamma,p}$ on a nucleus (Z, A) can be expressed as:

$$\lambda_{(\gamma,p)} = \frac{2G_f}{G_i}\left(\frac{\mu k_B T}{2\pi\hbar^2}\right)^{3/2}\lambda_{(p,\gamma)}\mathrm{e}^{-S_p/k_B T} \quad (1)$$

where S_p is the proton separation energy for the nucleus (Z, A), μ is the reduced mass of the target (nucleus of atomic mass number, A) and projectile (proton) system, G_i and G_f are the nuclear partition functions for the initial and final nuclei, T is the astrophysical temperature, $\lambda_{(p,\gamma)}$ is the proton capture rate on the forward reaction (i.e. on nucleus $(Z - 1, A)$), k_B is the Boltzmann constant, and $\hbar$ is the reduced Planck constant.

The exponential dependence on proton separation energies in Eq. 1 means that the abundance ratio between neighboring isotones $(Z - 1, N)$ and (Z, N) depends sensitively on their masses. This is even more emphasized at waiting-point nuclei, where the (p, γ) and (γ, p) reactions compete with the β^+ decay. As such, nuclear masses have a strong impact on the final elemental abundance of the rp process, also known as burst ashes. This is illustrated for the mass excess of ^{65}As in Fig. 2. In general, the mass-excesses should be known with a precision of better than 10 keV to better model the rp process [15].

For lighter rp-process nuclei, or near magic shell closures, the level density is rather low. There, the reaction rate is dominated by resonant proton captures on selected states at

excitation energies $E_{x,i}$ and the total resonant reaction rate can be calculated as a sum over all resonances i:

$$N_A\langle\sigma v\rangle = 1.5399 \times 10^{11}\,(\mu T_9)^{-3/2} \times \sum_i (\omega\gamma)_i \exp\frac{-11.605(E_{x,i} - S_p)}{T_9} \quad (2)$$

where μ is the reduced mass for the reaction, T_9 is the temperature in GK, S_p is the proton separation energy of the final nucleus, and $\omega\gamma$ is the resonance strength. In order to accurately determine the resonant proton capture rates, the proton separation energy has to be precisely known in addition to the resonant state excitation energies. Often the proton separation energy introduces the largest uncertainty to the resonance energy $E_{res} = E_x - S_p$, and $\approx$ keV precision is desirable for the mass-excess values.

The type I x-ray burst ashes depend also on the formation of cycles at points where α separation energies become low and the material is cycled back via (p,α) or (γ,α) reactions. Examples of cycles in the rp process are the Ni-Cu [17], Zr-Nb [3], and SnSbTe [18] cycles. Of these, the SnSbTe cycle determines the endpoint of the rp process. The process cannot proceed to heavier nuclei due to the low alpha separation energies of the tellurium isotopes [18]. Even in extremely hydrogen-rich conditions, where the process can proceed beyond ^{56}Ni and ^{64}Ge, the heaviest burst ashes are located at $A \approx 110$ (see Fig. 2).

The burst ashes eventually fall into deeper layers of the neutron star crust, where superbursts can convert the ashes to nuclei in the iron-nickel region [19]. In even deeper layers, electron captures on nuclei drive the composition to more neutron-rich nuclei and release neutrinos. The electron captures can cool the crust via cycles of electron captures and β^- decays [20] but also strongly heat it, depending on their Q values and the depth in the crust [21]. The electron-capture Q values depend on the masses of the parent and daughter nuclei and the excitation energy of the final state in the daughter nucleus. Therefore, the masses of neutron-rich nuclei involved in the electron-capture processes in the accreting neutron star crust help to evaluate the resulting heat sources or heat sinks in the crust. In addition to accreting neutron stars, electron captures have been shown to play a role in core collapse supernovae (see e.g. Ref. [22]) and information on nuclear masses is similarly needed.

2.2 r process

The rapid neutron capture (r process) is an astrophysical process accountable for the production of the heaviest elements in nature. The astrophysical site of the r process remains an open question, with rare classes of supernovae and the merger of compact objects as leading candidates [23]. These sites are thought to provide a sufficient population of free neutrons that

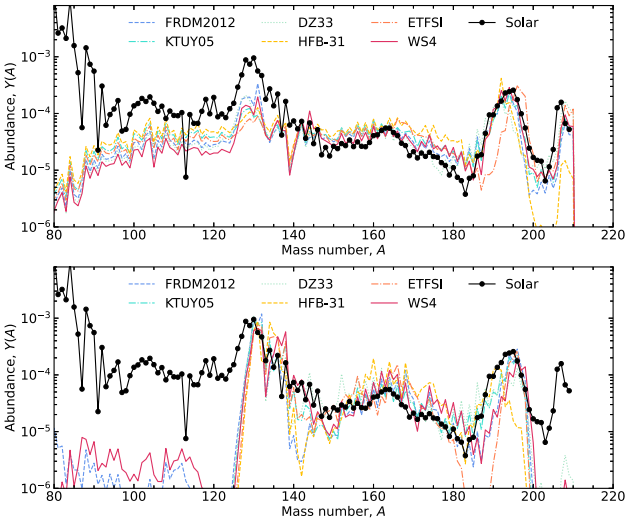

Fig. 3 The astrophysical r-process abundances using modern mass models in comparison with solar data. The top panel showcases extremely neutron-rich conditions of the dynamical ejecta from a neutron star merger. The bottom panel shows the conditions from an accretion disk wind with initial electron fraction of $Y_e = 0.20$

are used as building blocks to synthesize the heavier elements [24]. Here we briefly cover how the r process operates and the foundational role of masses in the theoretical treatment thereof; for recent reviews of the r process consult references [25–27].

The r process proceeds initially by the rapid capture of neutrons relative to the timescale for nuclear β-decay [28]. In this early stage, exceedingly short-lived nuclei are created for which there is limited to no experimental information [29]. Once the abundant population of free neutrons is consumed, the neutron-rich material decays into more long-lived species [30]. Each of these longer-lived species may have several independent measurements of their properties (e.g. masses, half-lives, excited states, and/or cross sections). The r process is estimated to last roughly a second from the initial capture of neutrons to the decay phase, producing characteristic abundance patterns found in old stars [31].

It is in the earliest stage of nucleosynthesis—during the rapid capture of neutrons—that theoretical masses must be employed. Such models are exceedingly robust in predicting the bulk behavior of nuclei [32–38]. However, these models have roughly a factor of 10 less precision than modern measurements, which propagates as a significant source of uncertainty [39]. Figure 3 highlights the range in astrophysical abundances using commonly employed mass models. Two possible candidate astrophysical conditions are shown: the dynamical and wind ejecta of a neutron star merger. The relative abundance of isotopes is displayed on the Y-axis versus atomic mass number, A, on the X-axis. Differences of one order of magnitude (or more) around the abundance peaks ($A \sim 130$ and $A \sim 195$) are indicative of the need for pre-

cise mass measurements. A reduction in uncertainty on the astrophysical r process abundances requires precision mass measurements for participating nuclei on the order of 50 keV or less. Given the clear relationship between atomic masses and simulated abundances, this motivates the need to answer the question: in what way do masses cause such large discrepancies?

Masses, in particular their differences, enter into simulations of the r process in numerous contexts [40,41]. Estimations of astrophysical reaction rates require a mass difference that defines the Q-value associated with the particular reaction [42]. For instance, with radiative neutron capture at astrophysical energies, the one neutron separation energy sets the bulk of the excitation energy in the compound system [43]. The one neutron separation energy also enters into the associated Q-value that is used via detailed balance in the calculation of photo-disintegration (inverse) rates associated with neutron capture. In like manner to the proton, the neutron photo-disintegration rate can be expressed via the equation,

$$\lambda_{(\gamma,n)} = \frac{2}{n_n}\frac{G'(T)}{G(T)}\left(\frac{\mu k_B T}{2\pi\hbar^2}\right)^{3/2}\lambda'_{(n,\gamma)}\mathrm{e}^{-S_n/k_B T} \tag{3}$$

where S_n is the neutron separation energy, μ is the reduced mass of the target (nucleus of atomic mass number, A) and projectile (neutron) system, the neutron density is given by n_n, $G(T)$ is the nuclear partition function, T is the astrophysical temperature, $\lambda_{(n,\gamma)}$ is the neutron capture rate of the forward reaction, and both k_B and $\hbar$ are physical constants. The primed quantities represent the nucleus with one fewer neutron relative to the unprimed quantities. Because S_n appears in the exponent, it has a profound influence in setting the photo-disintegration rate. For r-process nuclei, $m_A \gg m_n$, so the reduced mass effectively scales the photo-disintegration rate.

Mass differences also enter into decay properties, setting the energy window for β-decay (Q_β) along with the energy windows associated with delayed neutron emission [44,45]. These energy windows are critical for regulating delayed neutron emission probabilities and thus contribute to the final odd-even staggering found in r-process abundances [46].

Furthermore, mass differences impact certain properties unique to the heaviest nuclei that may be produced during the r process, in particular, rates of nuclear fission [47]. In such cases, the difference between the ground state mass and the mass of the system near the so-called saddle configuration sets the barrier height which approximates the resistance of the nucleus to undergo fission [48]. A nucleus with a small barrier readily undergoes fission while a large barrier is prohibitive. The interplay between the neutron separation energy and fission barrier is informative to regions that undergo neutron-induced fission, while the relative value of Q_β to fission barrier defines regions which may proceed via β-delayed fission [49]. In general, the lower the fission barrier, the more propensity there is for fission, including the possibility of spontaneous fission from the ground (or excited) state [50].

In addition to the impact of setting the values of astrophysical reactions rates, mass differences define the extent of the bound (and thus accessible) nuclei [51]. Masses further impact the estimation of energy release by participating reactions which is used in the computation of heating of r-process material [52]. This effect is important at early times which may impact the thermodynamic evolution of the astrophysical trajectory. At later times, the variation in heating coupled with abundance differences (as in Fig. 3) can influence light curve modeling [53,54]. The existence of these uncertainties compounds current difficulties in interpreting kilonova that can be observed in association with the merger of compact objects [55].

3 Mass measurement techniques

In the past few decades, the advent of new mass measurement devices and techniques has greatly enhanced the reach and precision of nuclide masses. These devices and techniques have been developed, in part, to address the challenges in obtaining mass measurements of nuclides relevant to astrophysics: having a sensitive device to get the precision required of hard-to-produce short-lived nuclides while minimizing systematic effects that arise from such things as impure ion samples. The following sections describe some of these devices and highlight how they overcome some of the challenges noted above.

3.1 TOF-Bρ

One method used to determine the mass of short-lived isotopes is to let the fast radioactive ions produced in a reaction travel over a long distance to a fast detector which records their time of arrival. Along the path, ions will spread out due to differences in energy and mass; the lighter ion will travel faster, the heavier ions slower, and for a relatively small energy spread the difference in time of arrival will be related to the mass difference. The energy spread introduced in the nuclear reaction producing these isotopes can be significant so that this method is best employed for radioactive ions produced by fragmentation reactions at high energy where the energy spread of the produced nuclei is small, and by adding a momentum determination along the path so that the leading broadening effect can be corrected. This method is call the TOF-Bρ [for Time-Of-Flight and momentum (Bρ inside a magnet) measurement] technique [56] and, for a long path of the order of 100 meters and well understood ion optical properties, a mass resolving power ($\frac{m}{\Delta m}$) of the order of 10,000

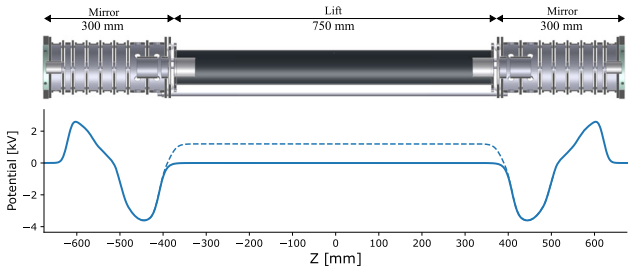

Fig. 4 A schematic of a MR-TOF which shows the electrostatic mirror electrodes on either side of a central lift electrode. The voltages applied to the electrodes form the potential gradient as displayed at the bottom, with the dashed line showing the voltages used to capture the ions and the solid line showing the voltages used to trap the ions

can be obtained. This method allows mass determination on the reaction products directly, without any preparation or conditioning, and is therefore applicable to the very shortest lived nuclei, with half-lives as short as a few hundred ns. Accuracy of the mass measurements is then limited by the statistics that can be accumulated, the presence of close calibration masses, and the stability of the system. Typical mass accuracy ranges from $\sim 10^{-5}$ to $\sim 10^{-6}$. This generally exceeds the required precision for astrophysics applications, but does provide access to the most exotic nuclei that cannot be reached by other methods.

3.2 MR-TOF

The TOF technique can be improved by making it independent of the energy dispersion of the beam. This is accomplished, and the device made more compact, by folding the long path via reflection between two electrostatic mirrors that are tuned to cancel out the dispersion in energy. The basic idea is shown in Fig. 4 where the voltage slope on the mirrors is such that the faster traversal of the center region by the higher energy ions is compensated by the extra distance they travel before being reflected in the electrostatic mirror. With the right electrostatic mirror slope, that total time equals that of lower energy ions that travel slower in between the mirrors but do not penetrate as far in them. That configuration is called a Multi-Reflection Time-Of-Flight (MR-TOF) spectrometer [57]. Well collimated short ion bunches at a few keV energy sent into such a device can bounce around for hundreds of turns, and a mass resolving power of the order of 100,000 can be achieved in tens of milliseconds. This is sufficient to separate most isobars and obtain mass differences from their time-of-flight differences.

This technique however requires the radioactive ions to be prepared as a cool low-energy beam with a small energy spread and a short pulse structure. This is typically done by first accumulating and cooling the ions in a radiofrequency (RF) buncher [58] and extracting them as an ion pulse with a tens-of-ns width. This process introduces some losses in the deceleration, capture, and cooling of the beam, in addition to introducing a time delay of the order of a few tens of ms for the cooling of the bunches and time in the MR-TOF. It is therefore applicable to isotopes with halflives down to tens of ms, or as low as a few ms if decay losses can be tolerated, and extremely low production yield. The mass accuracy can reach $\sim 10^{-7}$ if statistics is not a limitation and calibrants close in mass are available.

3.3 Storage ring

Other variations on the TOF technique can be obtained in storage rings for relativistic heavy-ions (see e.g. Ref. [59]). In this case, the long flight path is obtained with ions circulating repeatedly in a large circumference ring. Two main techniques are available in this case: the Schottky mass spectrometry [60] method and the multi-turn isochronous [61] mass measurement method. The multi-turn isochronous method uses fast beams directly after a fragment separator [62] which selects a subset of ions of interest and injects them into the ring. The ion optics of the ring is tuned such that the revolution time is as independent of the energy of the ions as possible. In this case, all ions of a given species have the same rotation frequency and the ratio of these frequencies for different species is related to the mass ratio for the highly-charged ions. The correction for the missing charges can be made quite accurately, and essentially no time is lost in beam preparation, so therefore this technique is also applicable to very short-lived isotopes. A mass accuracy of $\sim 10^{-6} - 10^{-7}$ can be reached by this method. A very recent development at Lanzhou where a $B\rho$ measurement is added in a technique called the $B\rho$-defined IMS, promises even higher precision [63,64]. The second method uses a different approach where, instead of reducing the influence of the energy spread, the energy spread itself is reduced. This is done by first injecting the relativistic ions of interest in the storage ring but then cooling these ions in an electron cooler section so that the velocity spread is all but eliminated. Each mass then takes a slightly different orbit in the ring, resulting in a mass dependent rotational frequency. That frequency is then measured by a non-destructive pick up system called a Schottky [65] detector. The mapping from frequency to mass can in principle be calculated, but is in practice derived from the known masses circulating in the ring together with the unknown masses of interest. Since the relative ions are cooled, the intrinsic resolution of this technique is high enough to separate high-lying isomers and the accuracy can reach below 10^{-7} when known calibrants are available. The method however requires time for the electron cooling to be completed which limits it to isotopes of slightly longer halflives.

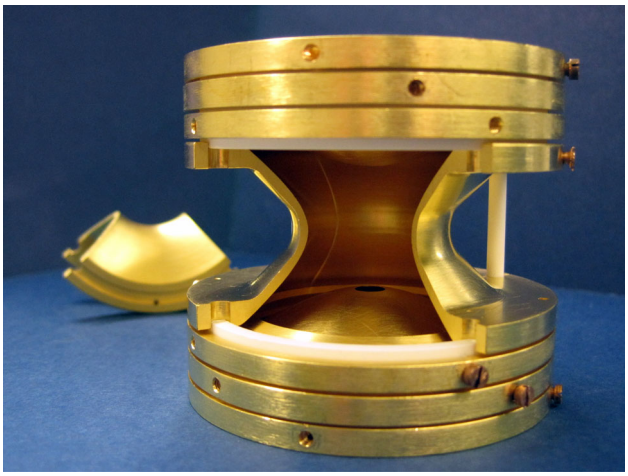

Fig. 5 Picture of the Canadian Penning trap, with one quadrant of the central ring electrode removed for illustrative purposes

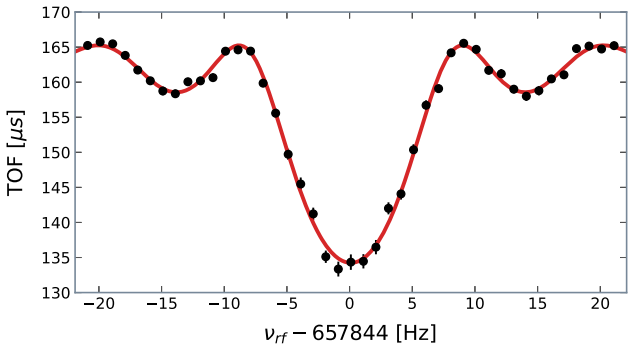

Fig. 6 A TOF-ICR measurement results in a fitted TOF spectrum as shown here for a measurement of $^{133}Cs^{+}$

3.4 Penning traps

Over the past few decades, Penning traps have become the preferred tool to make mass measurements of ions, where the mass m of an ion can be determined precisely via the measurement of the cyclotron frequency ν_c of that ion confined within a uniform, homogeneous magnetic field of strength B: $\nu_c = qB/m$, where q is the charge state of the ion. The most precise Penning trap measurements have been performed for stable ions, but precise mass measurements for hundreds of radioactive nuclei as short-lived as ^{11}Li ($t_{1/2}$ = 8.8 ms) have been measured [66].

The Penning trap itself is an electrode structure consisting of two endcap electrodes which describe hyperboloids of revolution and an intermediate ring electrode of hyperbolic cross-section [67]. A potential difference applied between the endcap electrodes and the ring electrode provides an axially harmonic electric potential along the magnetic field axis. In this manner, the ions can be trapped within the uniform field and their cyclotron frequency can be measured. The superposition of an electric field with the magnetic field results in the cyclotron frequency being split into two radial eigenfrequencies of motion that depend on the applied potential: a weakly mass dependent frequency ν_- (magnetron frequency), and a strongly mass dependent frequency ν_+ (reduced cyclotron frequency), such that $\nu_c = \nu_- + \nu_+$.

With the ring electrode split into four quadrants, as can be seen in Fig. 5, radiofrequency (RF) excitations can be applied. For applied dipole fields, the trapped ions are resonantly excited at their radial eigenfrequencies of motion (ν_+ and ν_-). For applied quadrupole fields, the trapped ions are resonantly excited at the sum of their eigenfrequencies ($2\nu_+$, $2\nu_-$, and $\nu_+ + \nu_- = \nu_c$). Given the cyclotron frequency is purely dependent on the uniform homogeneous magnetic field, and not on the electric field used to trap the ions, very precise measurements of the ion's mass can be made through a measurement of the ion's cyclotron frequency.

3.4.1 TOF-ICR

Over the past few decades, many of the precise mass measurements of radioactive nuclides have been made using the Time of Flight Ion Cyclotron Resonance (TOF-ICR) method [68], in which the radial energy gained through resonant excitations is transferred to linear energy as the ions drift adiabatically through the magnetic field gradient once ejected from the trap. To minimize systematic effects, the trapped ions are first subjected to a dipole field at the predominantly mass-independent magnetron frequency for a prescribed amount of time, establishing an orbital motion at a fixed radius. A quadrupole RF field excitation is then applied and, if the excitation is at the cyclotron frequency of the ions, a complete conversion from the initial magnetron motion to the higher frequency reduced cyclotron motion is accomplished [69,70]. This increase in radial energy can be seen as a reduction in the time of flight of the ions as they drift through the magnetic field gradient once ejected from the trap. By measuring the time of flight of the ions as a function of the applied quadrupole frequency, the cyclotron frequency can be determined by finding the minimum in the time-of-flight spectrum, as shown in Fig. 6.

With the TOF-ICR method, measurements of highest precision are obtained with ions of high charge state, low mass, and strong magnetic field strengths; but, for a given magnetic field and ion mass-to-charge during a typical experiment, higher precision measurements can be obtained by increasing the excitation time of the quadrupole field. This has the effect of narrowing the Fourier-limited width of the TOF spectrum, but this is ultimately limited by the half-life of the ions being studied. Having more statistics (more ions) also increases the precision of the measurement, but having more than one ion at a time in the trap can lead to systematic effects due to ion-ion interactions. Therefore, it is customary to limit the number of ions that are trapped, and instead to

repeat the scans of the applied cyclotron frequency until the desired precision is obtained.

Although a wealth of highly precise mass data has been gathered through TOF-ICR measurements, one of the limitations of this method is the effect of contaminant ions that are simultaneously trapped with the ions of interest. Not only does the presence of contaminant ions contribute to ion-ion interactions, but also the resulting TOF spectrum is affected through a reduction in its' depth at the resonant (cyclotron) frequency. This limitation was addressed by the relatively new phase-imaging ion-cyclotron-frequency technique (PI-ICR) described next.

3.4.2 PI-ICR

In 2013, a new technique to determine the cyclotron frequency was introduced [71]. This new method, whereby the radial ion motion of the trapped ions is effectively projected onto a position sensitive microchannel plate (MCP) detector, is now being implemented by many of the Penning trap facilities that once used the TOF-ICR method. The determination of the cyclotron frequency is accomplished by measuring the phase accumulation of the ions' orbital motion for a prescribed accumulation time. As with the TOF-ICR method, trapped ions are initially subjected to a dipole excitation, but this time at the reduced cyclotron frequency. A properly applied quadrupole field pulse fully converts the reduced cyclotron frequency to the lower magnetron frequency, and the ions subsequent ejection from the trap at a time, t_{tot}, later are projected onto the position sensitive MCP detector. This establishes an initial phase or reference spot. Subsequent ions trapped in the Penning trap are excited in a similar fashion, but with the quadrupole field applied at a time t_{acc} as to let the ions precess at its reduced cyclotron frequency and accumulate a phase relative to the initial phase. Then the ions are ejected at a time t_2 after the quadrupole field is applied, such that $t_{tot} = t_{acc} + t_2$. By measuring the accumulated phase, ϕ_c over the accumulation time interval, t_{acc}, the cyclotron frequency can be precisely determined, as shown in Fig. 7.

The PI-ICR technique has many advantages over the TOF-ICR technique. Foremost is the reduction in the effect from the presence of contaminant ions. Spots, from the ions' projection onto the MCP that are fully resolved from the spots resulting from contaminant ions, are negligibly affected by the contaminant ions, as opposed to the TOF spectrum from the TOF-ICR method. Another significant advantage is due to the fact that all ions with the PI-ICR technique are resonantly excited at the cyclotron frequency, as compared to the spectrum obtained from the TOF-ICR method where most of the data is off resonance. Thus, similar mass precision with the PI-ICR technique can be obtained with fewer overall ions than the TOF-ICR method. Finally, since it measures the phase of the cyclotron motion, not the frequency itself, it can yield higher resolution than the Fourier limit would normally allow.

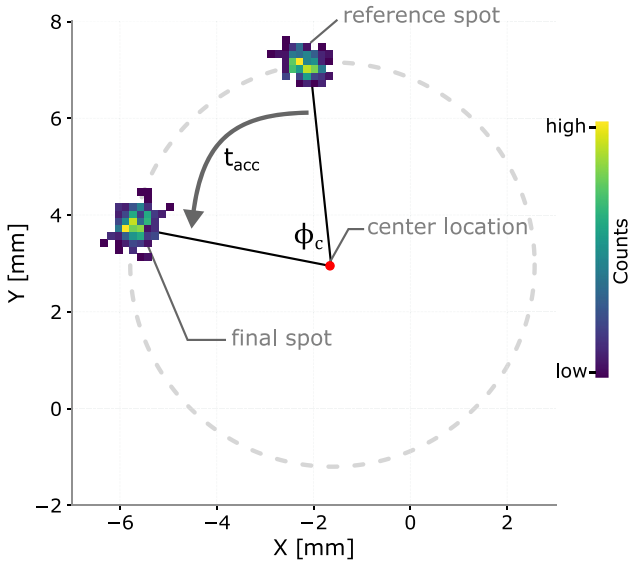

Fig. 7 An illustration of the PI-ICR technique, where the phase accumulation, ϕ_c, between a reference spot and final spot over a time of t_{acc} is used to determine the cyclotron frequency

4 Production of nuclides

Although stars can easily produce the nuclides of interest, having those nuclides available in the laboratory for measurements is not so trivial. And as is often the case, the most interesting nuclides to study are the most elusive. By using various reaction mechanisms, facilities around the world provide access to a large fraction of the nuclides of interest to astrophysics.

The most used reaction mechanisms in radioactive beam facilities are fragmentation and spallation, which are essentially the same reaction in different kinematics. In spallation, a light projectile, typically protons, hits a heavy target nucleus at a velocity well above that of individual nucleons in the nucleus. The target nucleus cannot react and rearrange itself fast enough to accommodate the extra energy and momentum, and some of its constituents are knocked off. The resulting reaction residue has little momentum impinged on it and is typically stopped in the target. The reaction product has to diffuse out of the target before being available for study and this diffusion is enhanced by keeping the target at very high temperature. This is the basis for the so-called ISOL method which saw its origin in many small laboratories but is now dominated by large facilities such as ISOLDE [72] at CERN and ISAC [73] at TRIUMF. The range of protons in material is very long so that enormous target thicknesses can be used resulting in, in principle, the highest production yield. The

diffusion and effusion out of the target is however dependent on the chemical properties of the produced isotopes and can introduce very long delays so that the extracted yield of the shortest lived isotopes is highly suppressed except for the most favorable chemical species.

Fragmentation proceeds in the opposite kinematics with relativistic heavy ions impinging on a light target. Again, the resulting collisions can knock out a number of nucleons from the incoming ions, but now the reaction product is moving at essentially the velocity and direction of the primary beam. This relatively well-behaved secondary beam can then be passed through a large separator where a combination of Bρ and energy loss selection [62] allows individual species to be separated in-flight, with essentially no delay. The target thickness available is again large, but the total number of beam particles is lower than what can be obtained with protons in spallation reactions, so that the overall production is lower but all products are extracted with high efficiency and no delays. This technique is the workhorse for the largest radioactive ion beam facilities such as RIBF [74], GSI [75] and FRIB [76].

Both fragmentation and spallation reactions can access effectively neutron-deficient isotopes and a large fraction of neutron-rich nuclides. For mid-mass neutron-rich nuclei, fission provides an additional very efficient production mechanism. This is typically done by proton irradiation of a uranium or thorium compound target at ISOL facilities, or by in-flight fission of a uranium beam at a fragmentation facility. The raw production is dominated by the fission yield of uranium, broadened somewhat by the extra energy brought in by the reaction initiating the fission. The relative production rates and extraction efficiencies are similar to those seen in spallation and fragmentation reactions, except maybe for the in-flight fission products being more difficult to separate than fragmentation products because of the extra momentum spread brought in by the fission reaction. Spontaneous fission can also be used to produce and extract fission fragments as is the case for example at the CARIBU facility at ANL [77], which uses spontaneous fission of ^{252}Cf and a rapid and universal extraction mechanism to provide a range of unique fission products that is shifted to higher masses by the heavier fissioning system. The unique extraction system provides access to all fission products, independently of their chemical properties, with exquisite ion optical properties at low energy.

Two final main reaction mechanisms involve nuclei colliding at velocities similar to those of the nucleons inside the nucleus. Fusion-evaporation fuses the two nuclei involved in the collision and gets rid of the excitation energy by emitting a few nucleons and gamma rays. This reaction mechanism is the bread and butter of Coulomb-barrier energy heavy-ion facilities and produces neutron-deficient isotopes and the heaviest isotopes. It also provides access to excited states in the nuclei of interest which can be of interest to astrophysical reactions. Finally, at energies slightly above the Coulomb barrier, multi-nucleon transfer reactions can take place which can populate regions that are difficult to populate with any other reaction mechanism. The region around the N=126 closed neutron shell, responsible for the formation of the heaviest r-process abundance peak, is an example. Collecting these reaction products is however very difficult because of the large angle of the production cone for this reaction. Facilities such as KISS [78] at KEK and the N=126 Factory [79] at ANL are leading the way in trying to use this approach to probe this region.

5 Results and highlights

Given the advances in facilities to deliver isotopes of interest, and the development of devices and techniques to precisely measure the masses of isotopes of relevance for astrophysics, the past couple of decades have seen a wealth of new measurements and have greatly increased our understanding of the various astrophysical processes observed in the universe. A summary of those measurements and highlights are presented here.

5.1 *rp* process

As discussed in Sect. 2.1, waiting-point nuclides are of special interest for the rp process. The masses for most of the waiting-point nuclides in the rp process have been determined via Penning-trap mass spectrometry during the last two decades. The masses of ^{56}Ni [80] and ^{60}Zn [80] were measured at JYFLTRAP, ^{64}Ge [81] and ^{68}Se [82] at CPT, ^{72}Kr [83] and ^{76}Sr [84] at ISOLTRAP, and both ^{64}Ge [85] and ^{80}Zr [86] at LEBIT.

The heaviest waiting-point nuclides in the rp process have remained inaccessible for precision mass measurements. The mass of ^{92}Pd is based on its Q_{EC} value determined via decay spectroscopy [87] and the ^{92}Rh mass measurements [88,89]. The masses of ^{84}Mo, ^{88}Ru, and ^{96}Cd are still based on extrapolations in the latest Atomic Mass Evaluation (AME20) [90], and should be explored at radioactive beam facilities in the near future.

The region around the Ni-Cu cycle and the waiting-point nucleus ^{56}Ni has been studied via mass spectrometry in detail, see e.g. Refs. [80,91]. There the main question is whether the bypass routes via ^{55}Ni$(p,\gamma)^{56}$Cu$(p,\gamma)^{57}$Zn $(\beta^+)^{57}$Cu or ^{56}Ni$(p,\gamma)^{57}$Cu$(p,\gamma)^{58}$Zn$(\beta^+)^{58}$Cu can compete favorably against the slow beta decay of ^{56}Ni ($t_{1/2}$ = 6.095 d). The mass of ^{57}Zn is still experimentally unknown, and the mass excess of ^{58}Zn is based on an ^{58}Ni$(\pi^+,\pi^-)^{58}$Zn experiment [92] with an uncertainty of 50 keV.

Recent mass measurements performed using the isochronous mass spectrometry at the storage ring in Lanzhou [93] showed that ^{81}Zr and ^{83}Nb are significantly less bound than reported earlier. These results do not favor a strong Zr-Nb cycle; however, the mass of ^{84}Mo is still based on extrapolations.

The endpoint of the *rp* process is in the $A \approx 110$ region, where the SnSbTe cycle [18] takes place. The precision mass measurements in the SnSbTe region [94] have shown that this cycle is not as strong as originally considered. The strongest cycle proceeds via $^{106}\mathrm{Sn}(p,\gamma)^{107}\mathrm{Sb}(p,\gamma)^{108}\mathrm{Te}(\gamma,\alpha)^{104}\mathrm{Sn}$, with only about 13 % branch at ^{106}Sn. Thus, most of the proposed cycles in the *rp* process have turned out to be not as strong as originally predicted.

Sensitivity studies reported around a decade ago [5,13] highlighted around 20 nuclides for which the mass-excess value should be experimentally determined or precision improved. Since then, many of the proposed nuclides have been measured via precision mass spectrometry, such as ^{31}Cl [95], ^{46}Mn [96], ^{56}Cu [91], ^{61}Ga [97], ^{71}Br [98], ^{84}Nb [99], ^{89}Ru [99] and ^{99}In [100]. As a result, a more recent sensitivity study [14] could only indicate the mass uncertainties of ^{27}P, ^{61}Ga, and ^{65}As as having a significant impact on the calculated light curves of normal type I x-ray bursts. Of these, ^{61}Ga has been measured at TRIUMF [97] and the mass of ^{27}P has been determined via beta-delayed protons of ^{27}S [101]. Thus, the only remaining main uncertainty is the mass of ^{65}As.

The masses of ^{80}Zr, ^{81}Zr, and ^{82}Nb were found to have an effect on the final composition of the burst ashes in Ref. [14]. Of these, ^{80,81}Zr have been recently measured at LEBIT and only ^{82}Nb remains to be measured. For extreme x-ray bursts extending up to heaviest masses, the remaining mass uncertainties come from ^{58}Zn, ^{62}Ge, ^{65}As, ^{66}Se, ^{78}Y, ^{79}Zr, ^{82}Nb, ^{86}Tc, ^{91}Rh, and ^{95}Ag [14], after taking into account the recent progress in the mass measurements. In addition to the measurements mentioned above, the neutron-deficient indium masses have been reported in Ref. [102]. The ^{98}Cd mass has been improved via decay spectroscopy [87] but a direct mass measurement is still missing.

Tremendous progress has been made in the mass values of neutron-deficient nuclides during the last two decades. Although only a few key nuclides are remaining to be measured for the *rp* process light curve and abundance calculations, high-precision mass measurements can help to constrain resonant proton capture reaction rates. For such studies, a precision of around a few keV is required in the mass-excess value. For example, the $^{23}\mathrm{Al}(p,\gamma)^{24}$Si reaction rate has been recently constrained via the mass measurement of ^{24}Si in [103]. With better production rates at radioactive beam facilities, more exotic proton-capture reactions can be studied and their resonance energies constrained via high-precision mass measurements in the future.

For the electron-capture processes taking place in the deeper layers of the neutron star crust, TOF-Bρ mass spectrometry [104,105] has provided new mass values for many neutron-rich nuclei in the argon to nickel region [21,106]. Although the precision is far from Penning-trap mass spectrometry, the TOF-Bρ measurements extend the limits of known mass surface and provide initial mass values for nuclear astrophysics calculations. For example, the TOF-Bρ measurements showed that the Q value for $^{66}\mathrm{Fe}\rightarrow{}^{66}$Mn electron captures was 2.1 MeV (2.6σ) lower than predicted, indicating that these transitions take place closer to the surface than expected [21]. Further Penning-trap mass measurements can help to improve the calibrations, and therefore the accuracy, of the TOF-Bρ experiments.

5.2 *r* process

Sensitivity studies summarize the impact of various physical quantities to relevant observables in astrophysical environments. Because masses influence predictions of nearly every nuclear quantity relevant to the *r*-process, there are different levels of sophistication in studying their wide-ranging effects. Propagating changes to masses to separation energies, as in Eq. 3, is one way to understand the impact of masses [107,108]. Advanced propagation techniques recalculate more properties (including e.g. neutron capture rates) to give a more robust estimate of mass changes on abundance patterns [42,109,110]. Monte Carlo techniques may also be used to uncover the correlations between masses and abundance patterns [111–115]. Sensitivity studies of individual mass changes for main *r* process conditions have been summarized in Ref. [116].

A recent measurement of the mass of ^{123}Pd using the Rare-RI Ring at RIKEN [117] has verified the predictions of sensitivity studies—that a single mass change can have substantial impact on final abundances. In the case of ^{123}Pd, a nucleus near the $N = 82$ shell closure, a variety of different astrophysical conditions were studied and it was shown that when combined together the new mass measurement improves the match to the solar pattern. The impact of the new ^{123}Pd mass measurement is shown as a function of electron fraction in Fig. 8.

Masses of highly-deformed, neutron-rich nuclei are of special interest to simulations of *r* process nucleosynthesis as they can be used to diagnose the astrophysical conditions present when these elements are synthesized [118,119]. This work led to the idea that the properties of neutron-rich nuclei can be used to 'reverse engineer' the masses of rare earth nuclei that may cause the pygmy bump in the abundance pattern around mass number, $A \sim 165$ [120,121]. Thus far, measurements have been in line with conditions that are favorable for a 'hot' *r*-process environment that has a sustained equilibrium phase between neutron captures and

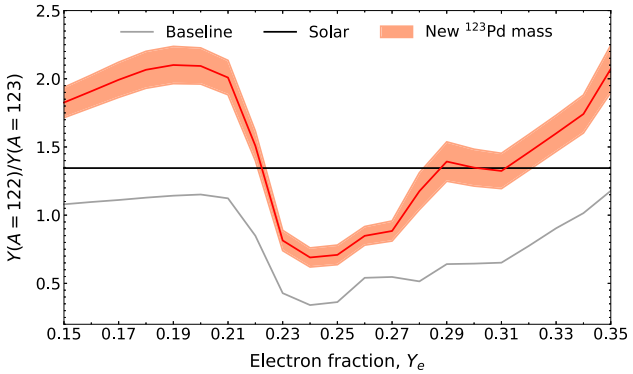

Fig. 8 The impact of the new ^{123}Pd mass measurement on the local *r* process abundances across a range of conditions (indicated by electron fractions). The default calculation is in grey. The new mass measurement (red) moves the simulated abundances closer to the solar value (black line). Calculations from Ref. [117]

photo-disintegration [122–125]. Future measurements in this region should be extended to sufficiently neutron-rich nuclei to either confirm a nuclear structure origin of the rare earth peak, or indicate another process, such as fission recycling, may be responsible [114,126–128].

Excited states also play an influential role in the *r* process as they help to set associated rates [129]. Nuclear isomers may also be populated during the radioactive decay of *r*-process species [130]. Such isomers may become astrophysically metastable or an astromer [131], in which case they can impact nucleosynthetic and observational outcomes [132]. The resolution of excited state energies, is an important component in determining whether a nuclear isomer may be an astromer. An example from Ref. [132] is the case of ^{128m}Sb which can accelerate nuclear flow back to stability if populated. Preliminary sensitivity studies of *r*-process astromers pinpoint where future experimental efforts are warranted [133].

The need to incorporate precision data, along with well-quantified uncertainties has prompted researchers to begin exploring Machine Learning (ML) techniques to predict unknown masses. Gaussian processes have been used to combine different mass model predictions together [134] and to quantify the limits of the nuclear landscape [135]. Most recently, probabilistic ML models such as the Mixture Density Network have been shown to support predictions of masses and uncertainties simultaneously [136]. When combined with physics-informed constraints, these ML models are capable of precise predictions using a fraction of known data [137].

6 Concluding remarks

The advances in mass measurement devices and techniques have yielded a substantial growth of precise mass data which has greatly improved our understanding of astrophysical processes. Although many of the masses involved in the astrophysical *rp* process have now been measured, some of the finer details and the nature of neutron star crusts could still benefit from the mass measurement of some key nuclei. As for the astrophysical *r* process, progress has been made in describing the origins of such features as the rare-earth peak in the solar abundance pattern, but many nuclei involved in the formation of the third *r*-process peak at A∼195 and nuclei that actively participate in rapid neutron capture are only now becoming within reach of measurement. In the coming years mass measurements of neutron-rich nuclei may help to answer one of the most challenging questions in physics: what is the origin of the heavy elements within the universe?

Acknowledgements This work was funded by the U.S. Department of Energy, Office of Nuclear Physics, under Award No. DE-AC02-06CH11357 (ANL). M.R.M. was supported by the U.S. Department of Energy through the Los Alamos National Laboratory. Los Alamos National Laboratory is operated by Triad National Security, LLC, for the National Nuclear Security Administration of the U.S. Department of Energy (Contract No. 89233218CNA000001). A.K. acknowledges support from the European Union's Horizon 2020 research and innovation programme under grant agreement No 771036 (ERC CoG MAIDEN).

Data Availability Statement This manuscript has no associated data or the data will not be deposited. [Authors' comment: This review covers previously published data and these published works are cited].

References

1. E.M. Burbidge, G.R. Burbidge, W.A. Fowler, F. Hoyle, Rev. Mod. Phys. **29**, 547 (1957). https://doi.org/10.1103/RevModPhys.29.547
2. R.K. Wallace, S.E. Woosley, Astrophys. J. Suppl. Ser. **45**, 389 (1981). https://doi.org/10.1086/190717
3. H. Schatz, A. Aprahamian, J. Görres, M. Wiescher, T. Rauscher, J. Rembges, F.K. Thielemann, B. Pfeiffer, P. Möller, K.L. Kratz, H. Herndl, B. Brown, H. Rebel, Phys. Rep. **294**, 167 (1998). https://doi.org/10.1016/S0370-1573(97)00048-3
4. J. Grindlay, H. Gursky, H. Schnopper, D.R. Parsignault, J. Heise, A.C. Brinkman, J. Schrijver, Astrophys. J. Lett. **205**, L127 (1976). https://doi.org/10.1086/182105
5. A. Parikh, J. José, G. Sala, C. Iliadis, Prog. Part. Nucl. Phys. **69**, 225 (2013). https://doi.org/10.1016/j.ppnp.2012.11.002
6. C. Fröhlich, G. Martínez-Pinedo, M. Liebendörfer, F.K. Thielemann, E. Bravo, W.R. Hix, K. Langanke, N.T. Zinner, Phys. Rev. Lett. **96**, 142502 (2006). https://doi.org/10.1103/PhysRevLett.96.142502
7. J. Pruet, R.D. Hoffman, S.E. Woosley, H.T. Janka, R. Buras, Astrophys. J. **644**, 1028 (2006). https://doi.org/10.1086/503891
8. T. Güver, Z.F. Bostancı, T. Boztepe, E. Gögü, P. Bult, U. Kashyap, M. Chakraborty, D.R. Ballantyne, R.M. Ludlam, C. Malacaria, G.K. Jaisawal, T.E. Strohmayer, S. Guillot, M. Ng, Astrophys. J. **935**, 154 (2022). https://doi.org/10.3847/1538-4357/ac8106
9. D.K. Galloway, M.P. Muno, J.M. Hartman, D. Psaltis, D. Chakrabarty, Astrophys. J. Suppl. Ser. **179**, 360 (2008). https://doi.org/10.1086/592044

10. D.K. Galloway, L. Keek, *Timing neutron stars: pulsations, oscillations and explosions* (Springer Berlin Heidelberg, ., 2020), p.209. https://doi.org/10.1007/978-3-662-62110-3_5
11. T. Güver, T. Boztepe, D.R. Ballantyne, Z.F. Bostanc, P. Bult, G.K. Jaisawal, E. Göğü, T.E. Strohmayer, D. Altamirano, S. Guillot, D. Chakrabarty, Mon. Not. R. Astron. Soc. **510**, 1577 (2021). https://doi.org/10.1093/mnras/stab3422
12. R.H. Cyburt, A.M. Amthor, A. Heger, E. Johnson, L. Keek, Z. Meisel, H. Schatz, K. Smith, Astrophys. J. **830**, 55 (2016). https://doi.org/10.3847/0004-637x/830/2/55
13. A. Parikh, J. José, C. Iliadis, F. Moreno, T. Rauscher, Phys. Rev. C **79**, 045802 (2009). https://doi.org/10.1103/PhysRevC.79.045802
14. H. Schatz, W.J. Ong, Astrophys. J. **844**, 139 (2017). https://doi.org/10.3847/1538-4357/aa7de9
15. H. Schatz, Int. J. Mass Spectrom. **251**, 293 (2006). https://doi.org/10.1016/j.ijms.2006.02.014
16. M. Wang, G. Audi, A. Wapstra, F. Kondev, M. MacCormick, X. Xu, B. Pfeiffer, Chin. Phys. C **36**, 1603 (2012). https://doi.org/10.1088/1674-1137/36/12/003
17. L. van Wormer, J. Görres, C. Iliadis, M. Wiescher, F.K. Thielemann, Astrophys. J. **432**, 326 (1994). https://doi.org/10.1086/174572
18. H. Schatz, A. Aprahamian, V. Barnard, L. Bildsten, A. Cumming, M. Ouellette, T. Rauscher, F.K. Thielemann, M. Wiescher, Phys. Rev. Lett. **86**, 3471 (2001). https://doi.org/10.1103/PhysRevLett.86.3471
19. A. Cumming, L. Bildsten, Astrophys. J. **559**, L127 (2001). https://doi.org/10.1086/323937
20. H. Schatz, S. Gupta, P. Möller, M. Beard, E.F. Brown, A.T. Deibel, L.R. Gasques, W.R. Hix, L. Keek, R. Lau, A.W. Steiner, M. Wiescher, Nature **505**, 62 (2013). https://doi.org/10.1038/nature12757
21. A. Estradé, M. Matoš, H. Schatz, A.M. Amthor, D. Bazin, M. Beard, A. Becerril, E.F. Brown, R. Cyburt, T. Elliot, A. Gade, D. Galaviz, S. George, S.S. Gupta, W.R. Hix, R. Lau, G. Lorusso, P. Möller, J. Pereira, M. Portillo, A.M. Rogers, D. Shapira, E. Smith, A. Stolz, M. Wallace, M. Wiescher, Phys. Rev. Lett. **107**, 172503 (2011). https://doi.org/10.1103/PhysRevLett.107.172503
22. C. Sullivan, E. O'Connor, R.G.T. Zegers, T. Grubb, S.M. Austin, Astrophys. J. **816**, 44 (2015). https://doi.org/10.3847/0004-637X/816/1/44
23. F.K. Thielemann, A. Arcones, R. Käppeli, M. Liebendörfer, T. Rauscher, C. Winteler, C. Fröhlich, I. Dillmann, T. Fischer, G. Martinez-Pinedo, K. Langanke, K. Farouqi, K.L. Kratz, I. Panov, I.K. Korneev, Prog. Part. Nucl. Phys. **66**, 346 (2011). https://doi.org/10.1016/j.ppnp.2011.01.032
24. C. Freiburghaus, S. Rosswog, F.K. Thielemann, Astrophys. J. **525**, L121 (1999). https://doi.org/10.1086/312343
25. T. Kajino, W. Aoki, A. Balantekin, R. Diehl, M. Famiano, G. Mathews, Prog. Part. Nucl. Phys. **107**, 109 (2019). https://doi.org/10.1016/j.ppnp.2019.02.008
26. C. Kobayashi, A.I. Karakas, M. Lugaro, Astrophys. J. **900**, 179 (2020). https://doi.org/10.3847/1538-4357/abae65
27. A. Arcones, F.K. Thielemann, Astron. Astrophys. Rev. **31**, 1 (2023). https://doi.org/10.1007/s00159-022-00146-x
28. J.J. Cowan, C. Sneden, J.E. Lawler, A. Aprahamian, M. Wiescher, K. Langanke, G. Martínez-Pinedo, F.K. Thielemann, Rev. Mod. Phys. **93**, 015002 (2021). https://doi.org/10.1103/RevModPhys.93.015002
29. W. Hillebrandt, Space Sci. Rev. **21**, 639 (1978). https://doi.org/10.1007/BF00186236
30. G.J. Mathews, R.A. Ward, Rep. Prog. Phys. **48**, 1371 (1985). https://doi.org/10.1088/0034-4885/48/10/002
31. I.U. Roederer, J.J. Cowan, A.I. Karakas, K.L. Kratz, M. Lugaro, J. Simmerer, K. Farouqi, C. Sneden, Astrophys. J. **724**, 975 (2010). https://doi.org/10.1088/0004-637X/724/2/975
32. Y. Aboussir, J. Pearson, A. Dutta, F. Tondeur, Nucl. Phys. A **549**, 155 (1992). https://doi.org/10.1016/0375-9474(92)90038-L
33. Y. Aboussir, J.M. Pearson, A.K. Dutta, F. Tondeur, At. Data Nucl. Data Tables **61**, 127 (1995). https://doi.org/10.1016/S0092-640X(95)90014-4
34. J. Duflo, A. Zuker, Phys. Rev. C **52**, R23 (1995). https://doi.org/10.1103/PhysRevC.52.R23
35. H. Koura, T. Tachibana, M. Uno, M. Yamada, Prog. Theor. Phys. **113**, 305 (2005). https://doi.org/10.1143/PTP.113.305
36. M. Liu, N. Wang, Y. Deng, X. Wu, Phys. Rev. C **84**, 014333 (2011). https://doi.org/10.1103/PhysRevC.84.014333
37. S. Goriely, N. Chamel, J.M. Pearson, Phys. Rev. C **88**, 024308 (2013). https://doi.org/10.1103/PhysRevC.88.024308
38. P. Möller, A. Sierk, T. Ichikawa, H. Sagawa, At. Data Nucl. Data Tables **109–110**, 1 (2016). https://doi.org/10.1016/j.adt.2015.10.002
39. E.M. Holmbeck, T.M. Sprouse, M.R. Mumpower, Eur. Phys. J. A **59**, 28 (2023). https://doi.org/10.1140/epja/s10050-023-00927-7
40. R. Surman, M. Mumpower, A. Aprahamian, Acta Phys. Pol. B **47**, 673 (2016). https://doi.org/10.5506/APhysPolB.47.673
41. R. Surman, M. Mumpower, EPJ Web Conf. **178**, 04002 (2018). https://doi.org/10.1051/epjconf/201817804002
42. D. Martin, A. Arcones, W. Nazarewicz, E. Olsen, Phys. Rev. Lett. **116**, 121101 (2016). https://doi.org/10.1103/PhysRevLett.116.121101
43. A. Couture, R.F. Casten, R.B. Cakirli, Nucl. Phys. News **29**, 18 (2019). https://doi.org/10.1080/10619127.2019.1642709
44. F. Minato, T. Marketin, N. Paar, Phys. Rev. C **104**, 044321 (2021). https://doi.org/10.1103/PhysRevC.104.044321
45. M.R. Mumpower, T. Kawano, T.M. Sprouse, Phys. Rev. C **106**, 065805 (2022). https://doi.org/10.1103/PhysRevC.106.065805
46. I. Dillmann, A. Tarifeño-Saldivia, Nucl. Phys. News **28**, 28 (2018). https://doi.org/10.1080/10619127.2018.1427937
47. M.R. Mumpower, P. Talou, R. Vogt, in *Nuclear fission: theories experiments and applications*. ed. by P. Talou, R. Vogt (Springer International Publishing, Cham, 2023), pp.401–464. https://doi.org/10.1007/978-3-031-14545-2_4
48. J.R. Nix, Annu. Rev. Nucl. Sci. **22**, 65 (1972). https://doi.org/10.1146/annurev.ns.22.120172.000433
49. P. Möller, A.J. Sierk, T. Ichikawa, A. Iwamoto, M. Mumpower, Phys. Rev. C **91**, 024310 (2015). https://doi.org/10.1103/PhysRevC.91.024310
50. A. Baran, M. Kowal, P.G. Reinhard, L. Robledo, A. Staszczak, M. Warda, Nucl. Phys. A **944**, 442 (2015). https://doi.org/10.1016/j.nuclphysa.2015.06.002
51. J. Erler, N. Birge, M. Kortelainen, W. Nazarewicz, E. Olsen, A.M. Perhac, M. Stoitsov, Nature **486**, 509 (2012). https://doi.org/10.1038/nature11188
52. J. Lippuner, L.F. Roberts, Astrophys. J. **815**, 82 (2015). https://doi.org/10.1088/0004-637X/815/2/82
53. Y.L. Zhu, T. Sprouse, M.R. Mumpower, N. Vassh, R. Surman, G.C. McLaughlin, in *Nuclei in the Cosmos XV*. ed. by A. Formicola, M. Junker, L. Gialanella, G. Imbriani (Springer International Publishing, Cham, 2019), pp.469–472. https://doi.org/10.1007/978-3-030-13876-9_92
54. Y.L. Zhu, K.A. Lund, J. Barnes, T.M. Sprouse, N. Vassh, G.C. McLaughlin, M.R. Mumpower, R. Surman, Astrophys. J. **906**, 94 (2021). https://doi.org/10.3847/1538-4357/abc69e
55. J. Barnes, Y.L. Zhu, K.A. Lund, T.M. Sprouse, N. Vassh, G.C. McLaughlin, M.R. Mumpower, R. Surman, Astrophys. J. **918**, 44 (2021). https://doi.org/10.3847/1538-4357/ac0aec
56. A. Gillibert, W. Mittig, L. Bianchi, A. Cunsolo, B. Fernandez, A. Foti, J. Gastebois, C. Grégoire, Y. Schutz, C.

Stephan, Phys. Lett. B **192**, 39 (1987). https://doi.org/10.1016/0370-2693(87)91138-5
57. R. Wolf, D. Beck, K. Blaum, C. Böhm, C. Borgmann, M. Breitenfeldt, F. Herfurth, A. Herlert, M. Kowalska, S. Kreim, D. Lunney, S. Naimi, D. Neidherr, M. Rosenbusch, L. Schweikhard, J. Stanja, F. Wienholtz, K. Zuber, Nucl. Instrum. Methods Phys. Res. Sect. A **686**, 82 (2012). https://doi.org/10.1016/j.nima.2012.05.067
58. F. Herfurth, J. Dilling, A. Kellerbauer, G. Bollen, S. Henry, H.J. Kluge, E. Lamour, D. Lunney, R. Moore, C. Scheidenberger, S. Schwarz, G. Sikler, J. Szerypo, Nucl. Instrum. Methods Phys. Res. Sect. A **469**, 254 (2001). https://doi.org/10.1016/s0168-9002(01)00168-1
59. B. Franzke, Nucl. Instrum. Methods Phys. Res. Sect. B **24–25**, 18 (1987). https://doi.org/10.1016/0168-583X(87)90583-0
60. Y.A. Litvinov, H. Geissel, T. Radon, F. Attallah, G. Audi, K. Beckert, F. Bosch, M. Falch, B. Franzke, M. Hausmann, M. Hellström, T. Kerscher, O. Klepper, H.J. Kluge, C. Kozhuharov, K.E.G. Löbner, G. Münzenberg, F. Nolden, Y.N. Novikov, W. Quint, Z. Patyk, H. Reich, C. Scheidenberger, B. Schlitt, M. Steck, K. Sümmerer, L. Vermeeren, M. Winkler, T. Winkler, H. Wollnik, Nucl. Phys. A **756**, 3 (2005). https://doi.org/10.1016/j.nuclphysa.2005.03.015
61. M. Hausmann, J. Stadlmann, F. Attallah, K. Beckert, P. Beller, F. Bosch, H. Eickhoff, M. Falch, B. Franczak, B. Franzke, H. Geissel, T. Kerscher, O. Klepper, H.J. Kluge, C. Kozhuharov, Y.A. Litvinov, K.E.G. Löbner, G. Münzenberg, N. Nankov, F. Nolden, Y.N. Novikov, T. Ohtsubo, T. Radon, H. Schatz, C. Scheidenberger, M. Steck, Z. Sun, H. Weick, H. Wollnik, Hyperfine Interact. **132**, 289 (2001). https://doi.org/10.1023/A:1011911720453
62. G. Münzenberg, Nucl. Instrum. Methods Phys. Res. Sect. B **70**, 265 (1992). https://doi.org/10.1016/0168-583X(92)95942-K
63. M. Wang, M. Zhang, X. Zhou, Y.H. Zhang, Y.A. Litvinov, H.S. Xu, R.J. Chen, H.Y. Deng, C.Y. Fu, W.W. Ge, H.F. Li, T. Liao, S.A. Litvinov, P. Shuai, J.Y. Shi, M. Si, R.S. Sidhu, Y.N. Song, M.Z. Sun, S. Suzuki, Q. Wang, Y.M. Xing, X. Xu, T. Yamaguchi, X.L. Yan, J.C. Yang, Y.J. Yuan, Q. Zeng, X.H. Zhou, Phys. Rev. C **106**, L051301 (2022). https://doi.org/10.1103/PhysRevC.106.L051301
64. M. Zhang, X. Zhou, M. Wang, Y.H. Zhang, Y.A. Litvinov, H.S. Xu, R.J. Chen, H.Y. Deng, C.Y. Fu, W.W. Ge, H.F. Li, T. Liao, S.A. Litvinov, P. Shuai, J.Y. Shi, R.S. Sidhu, Y.N. Song, M.Z. Sun, S. Suzuki, Q. Wang, Y.M. Xing, X. Xu, T. Yamaguchi, X.L. Yan, J.C. Yang, Y.J. Yuan, Q. Zeng, X.H. Zhou, Eur. Phys. J. A **59**, 27 (2023). https://doi.org/10.1140/epja/s10050-023-00928-6. arXiv:2209.05701
65. F. Nolden, Proc. DIPAC **01**, 6 (2001)
66. M. Smith, M. Brodeur, T. Brunner, S. Ettenauer, A. Lapierre, R. Ringle, V.L. Ryjkov, F. Ames, P. Bricault, G.W.F. Drake, P. Delheij, D. Lunney, F. Sarazin, J. Dilling, Phys. Rev. Lett. **101**, 202501 (2008). https://doi.org/10.1103/PhysRevLett.101.202501
67. L.S. Brown, G. Gabrielse, Rev. Mod. Phys. **58**, 233 (1986). https://doi.org/10.1103/RevModPhys.58.233
68. G. Gräff, H. Kalinowsky, J. Traut, Z. Phys. A At. Nucl. **297**, 35 (1980). https://doi.org/10.1007/BF01414243
69. M. König, G. Bollen, H.J. Kluge, T. Otto, J. Szerypo, Int. J. Mass Spectrom. Ion Processes **142**, 95 (1995). https://doi.org/10.1016/0168-1176(95)04146-C
70. G. Bollen, R. Moore, G. Savard, H. Stolzenberg, J. Appl. Phys. **68**, 4355 (1990). https://doi.org/10.1063/1.346185
71. S. Eliseev, K. Blaum, M. Block, C. Droese, M. Goncharov, E. Minaya Ramirez, D.A. Nesterenko, Y.N. Novikov, L. Schweikhard, Phys. Rev. Lett. **110**, 082501 (2013). https://doi.org/10.1103/PhysRevLett.110.082501
72. M.A. Fraser, Y. Kadi, A.P. Bernardes, Y. Blumenfeld, E. Bravin, S. Calatroni, R. Catherall, B. Goddard, D. Parchet, E. Siesling, W.V. Delsolaro, G. Vandoni, D. Voulot, L.R. Williams (2017). https://doi.org/10.48550/ARXIV.1707.05129
73. R.E. Laxdal, R.A. Baartman, P. Bricault, G. Dutto, R. Poirier, P. Schmor, G. Stanford, Nucl. Phys. A **701**, 647 (2002). https://doi.org/10.1016/S0375-9474(01)01660-8
74. Y. Yano, T. Motobayashi, Nucl. Phys. News **17**, 5 (2007). https://doi.org/10.1080/10506890701750368
75. N. Angert, B. Franzke, in *Challenges and Goals for Accelerators in the XXI Century*, ed. by S. Myers, O. Bruning. pp. 279–306. https://doi.org/10.1142/9789814436403_0017
76. C. Wrede, EPJ Web Conf. **93**, 07001 (2015). https://doi.org/10.1051/epjconf/20159307001
77. G. Savard, S. Baker, C. Davids, A. Levand, E. Moore, R. Pardo, R. Vondrasek, B. Zabransky, G. Zinkann, Nucl. Instrum. Methods Phys. Res. Sect. B **266**, 4086 (2008). https://doi.org/10.1016/j.nimb.2008.05.091
78. H. Miyatake, A.I.P. Conf, Proceedings **2319**, 080006 (2021). https://doi.org/10.1063/5.0036990
79. G. Savard, M. Brodeur, J.A. Clark, R.A. Knaack, A.A. Valverde, Nucl. Instrum. Methods Phys. Res. Sect. B **463**, 258 (2020). https://doi.org/10.1016/j.nimb.2019.05.024
80. A. Kankainen, V.V. Elomaa, T. Eronen, D. Gorelov, J. Hakala, A. Jokinen, T. Kessler, V.S. Kolhinen, I.D. Moore, S. Rahaman, M. Reponen, J. Rissanen, A. Saastamoinen, C. Weber, J. Äystö, Phys. Rev. C **82**, 034311 (2010). https://doi.org/10.1103/PhysRevC.82.034311
81. J.A. Clark, K.S. Sharma, G. Savard, A.F. Levand, J.C. Wang, Z. Zhou, B. Blank, F. Buchinger, J.E. Crawford, S. Gulick, J.K.P. Lee, D. Seweryniak, W. Trimble, Phys. Rev. C **75**, 032801 (2007). https://doi.org/10.1103/PhysRevC.75.032801
82. J.A. Clark, G. Savard, K.S. Sharma, J. Vaz, J.C. Wang, Z. Zhou, A. Heinz, B. Blank, F. Buchinger, J.E. Crawford, S. Gulick, J.K.P. Lee, A.F. Levand, D. Seweryniak, G.D. Sprouse, W. Trimble, Phys. Rev. Lett. **92**, 192501 (2004). https://doi.org/10.1103/PhysRevLett.92.192501
83. D. Rodríguez, G. Audi, J. Äystö, D. Beck, K. Blaum, G. Bollen, F. Herfurth, A. Jokinen, A. Kellerbauer, H.J. Kluge, V. Kolhinen, M. Oinonen, E. Sauvan, S. Schwarz, Nucl. Phys. A **769**, 1 (2006). https://doi.org/10.1016/j.nuclphysa.2006.02.001
84. G. Sikler, G. Audi, D. Beck, K. Blaum, G. Bollen, F. Herfurth, A. Kellerbauer, H.J. Kluge, D. Lunney, M. Oinonen, C. Scheidenberger, S. Schwarz, J. Szerypo, Nucl. Phys. A **763**, 45 (2005). https://doi.org/10.1016/j.nuclphysa.2005.08.014
85. P. Schury, C. Bachelet, M. Block, G. Bollen, D.A. Davies, M. Facina, C.M. Folden III., C. Guénaut, J. Huikari, E. Kwan, A. Kwiatkowski, D.J. Morrissey, R. Ringle, G.K. Pang, A. Prinke, J. Savory, H. Schatz, S. Schwarz, C.S. Sumithrarachchi, T. Sun, Phys. Rev. C **75**, 055801 (2007). https://doi.org/10.1103/PhysRevC.75.055801
86. A. Hamaker, E. Leistenschneider, R. Jain, G. Bollen, S.A. Giuliani, K. Lund, W. Nazarewicz, L. Neufcourt, C.R. Nicoloff, D. Puentes, R. Ringle, C.S. Sumithrarachchi, I.T. Yandow, Nat. Phys. **17**, 1408 (2021). https://doi.org/10.1038/s41567-021-01395-w
87. J. Park, R. Krücken, D. Lubos, R. Gernhäuser, M. Lewitowicz, S. Nishimura, D.S. Ahn, H. Baba, B. Blank, A. Blazhev, P. Boutachkov, F. Browne, I. Čeliković, G. de France, P. Doornenbal, T. Faestermann, Y. Fang, N. Fukuda, J. Giovinazzo, N. Goel, M. Górska, H. Grawe, S. Ilieva, N. Inabe, T. Isobe, A. Jungclaus, D. Kameda, G.D. Kim, Y.K. Kim, I. Kojouharov, T. Kubo, N. Kurz, Y.K. Kwon, G. Lorusso, K. Moschner, D. Murai, I. Nishizuka, Z. Patel, M.M. Rajabali, S. Rice, H. Sakurai, H. Schaffner, Y. Shimizu, L. Sinclair, P.A. Söderström, K. Steiger, T. Sumikama, H. Suzuki, H. Takeda, Z. Wang, H. Watanabe, J. Wu, Z.Y. Xu, Phys. Rev. C **99**, 034313 (2019). https://doi.org/10.1103/PhysRevC.99.034313
88. C. Weber, V.V. Elomaa, R. Ferrer, C. Fröhlich, D. Ackermann, J. Äystö, G. Audi, L. Batist, K. Blaum, M. Block, A. Chaudhuri, M. Dworschak, S. Eliseev, T. Eronen, U. Hager, J. Hakala, F. Her-

furth, F.P. Heßberger, S. Hofmann, A. Jokinen, A. Kankainen, H.J. Kluge, K. Langanke, A. Martín, G. Martínez-Pinedo, M. Mazzocco, I.D. Moore, J.B. Neumayr, Y.N. Novikov, H. Penttilä, W.R. Plaß, A.V. Popov, S. Rahaman, T. Rauscher, C. Rauth, J. Rissanen, D. Rodríguez, A. Saastamoinen, C. Scheidenberger, L. Schweikhard, D.M. Seliverstov, T. Sonoda, F.K. Thielemann, P.G. Thirolf, G.K. Vorobjev, Phys. Rev. C **78**, 054310 (2008). https://doi.org/10.1103/PhysRevC.78.054310

89. J. Fallis, J.A. Clark, K.S. Sharma, G. Savard, F. Buchinger, S. Caldwell, A. Chaudhuri, J.E. Crawford, C.M. Deibel, S. Gulick, A.A. Hecht, D. Lascar, J.K.P. Lee, A.F. Levand, G. Li, B.F. Lundgren, A. Parikh, S. Russell, M. Scholte-van de Vorst, N.D. Scielzo, R.E. Segel, H. Sharma, S. Sinha, M.G. Sternberg, T. Sun, I. Tanihata, J. Van Schelt, J.C. Wang, Y. Wang, C. Wrede, Z. Zhou, Phys. Rev. C **84**, 045807 (2011). https://doi.org/10.1103/PhysRevC.84.045807
90. M. Wang, W. Huang, F. Kondev, G. Audi, S. Naimi, Chin. Phys. C **45**, 030003 (2021). https://doi.org/10.1088/1674-1137/abddaf
91. A.A. Valverde, M. Brodeur, G. Bollen, M. Eibach, K. Gulyuz, A. Hamaker, C. Izzo, W.J. Ong, D. Puentes, M. Redshaw, R. Ringle, R. Sandler, S. Schwarz, C.S. Sumithrarachchi, J. Surbrook, A.C.C. Villari, I.T. Yandow, Phys. Rev. Lett. **120**, 032701 (2018). https://doi.org/10.1103/PhysRevLett.120.032701
92. K.K. Seth, S. Iversen, M. Kaletka, D. Barlow, A. Saha, R. Soundranayagam, Phys. Lett. B **173**, 397 (1986). https://doi.org/10.1016/0370-2693(86)90402-8
93. Y. Xing, K. Li, Y. Zhang, X. Zhou, M. Wang, Y. Litvinov, K. Blaum, S. Wanajo, S. Kubono, G. Martínez-Pinedo, A. Sieverding, R. Chen, P. Shuai, C. Fu, X. Yan, W. Huang, X. Xu, X. Tang, H. Xu, T. Bao, X. Chen, B. Gao, J. He, Y. Lam, H. Li, J. Liu, X. Ma, R. Mao, M. Si, M. Sun, X. Tu, Q. Wang, J. Yang, Y. Yuan, Q. Zeng, P. Zhang, X. Zhou, W. Zhan, S. Litvinov, G. Audi, T. Uesaka, Y. Yamaguchi, T. Yamaguchi, A. Ozawa, C. Fröhlich, T. Rauscher, F.K. Thielemann, B. Sun, Y. Sun, A. Dai, F. Xu, Phys. Lett. B **781**, 358 (2018). https://doi.org/10.1016/j.physletb.2018.04.009
94. V.V. Elomaa, G.K. Vorobjev, A. Kankainen, L. Batist, S. Eliseev, T. Eronen, J. Hakala, A. Jokinen, I.D. Moore, Y.N. Novikov, H. Penttilä, A. Popov, S. Rahaman, J. Rissanen, A. Saastamoinen, H. Schatz, D.M. Seliverstov, C. Weber, J. Äystö, Phys. Rev. Lett. **102**, 252501 (2009). https://doi.org/10.1103/PhysRevLett.102.252501
95. A. Kankainen, L. Canete, T. Eronen, J. Hakala, A. Jokinen, J. Koponen, I.D. Moore, D. Nesterenko, J. Reinikainen, S. Rinta-Antila, A. Voss, J. Äystö, Phys. Rev. C **93**, 041304 (2016). https://doi.org/10.1103/PhysRevC.93.041304
96. C.Y. Fu, Y.H. Zhang, M. Wang, X.H. Zhou, Y.A. Litvinov, K. Blaum, H.S. Xu, X. Xu, P. Shuai, Y.H. Lam, R.J. Chen, X.L. Yan, X.C. Chen, J.J. He, S. Kubono, M.Z. Sun, X.L. Tu, Y.M. Xing, Q. Zeng, X. Zhou, W.L. Zhan, S. Litvinov, G. Audi, T. Uesaka, T. Yamaguchi, A. Ozawa, B.H. Sun, Y. Sun, F.R. Xu, Phys. Rev. C **102**, 054311 (2020). https://doi.org/10.1103/PhysRevC.102.054311
97. S.F. Paul, J. Bergmann, J.D. Cardona, K.A. Dietrich, E. Dunling, Z. Hockenbery, C. Hornung, C. Izzo, A. Jacobs, A. Javaji, B. Kootte, Y. Lan, E. Leistenschneider, E.M. Lykiardopoulou, I. Mukul, T. Murböck, W.S. Porter, R. Silwal, M.B. Smith, J. Ringuette, T. Brunner, T. Dickel, I. Dillmann, G. Gwinner, M. MacCormick, M.P. Reiter, H. Schatz, N.A. Smirnova, J. Dilling, A.A. Kwiatkowski, Phys. Rev. C **104**, 065803 (2021). https://doi.org/10.1103/PhysRevC.104.065803
98. J. Savory, P. Schury, C. Bachelet, M. Block, G. Bollen, M. Facina, C.M. Folden, C. Guénaut, E. Kwan, A.A. Kwiatkowski, D.J. Morrissey, G.K. Pang, A. Prinke, R. Ringle, H. Schatz, S. Schwarz, C.S. Sumithrarachchi, Phys. Rev. Lett. **102**, 132501 (2009). https://doi.org/10.1103/PhysRevLett.102.132501
99. M. Vilén, A. Kankainen, P. Baczyk, L. Canete, J. Dobaczewski, T. Eronen, S. Geldhof, A. Jokinen, M. Konieczka, J. Kostensalo, I.D. Moore, D.A. Nesterenko, H. Penttilä, I. Pohjalainen, M. Reponen, S. Rinta-Antila, A. de Roubin, W. Satuła, J. Suhonen, Phys. Rev. C **100**, 054333 (2019). https://doi.org/10.1103/PhysRevC.100.054333
100. M. Mougeot, D. Atanasov, J. Karthein, R.N. Wolf, P. Ascher, K. Blaum, K. Chrysalidis, G. Hagen, J.D. Holt, W.J. Huang, G.R. Jansen, I. Kulikov, Y.A. Litvinov, D. Lunney, V. Manea, T. Miyagi, T. Papenbrock, L. Schweikhard, A. Schwenk, T. Steinsberger, S.R. Stroberg, Z.H. Sun, A. Welker, F. Wienholtz, S.G. Wilkins, K. Zuber, Nat. Phys. **17**, 1099 (2021). https://doi.org/10.1038/s41567-021-01326-9
101. L.J. Sun, X.X. Xu, C.J. Lin, J. Lee, S.Q. Hou, C.X. Yuan, Z.H. Li, J. José, J.J. He, J.S. Wang, D.X. Wang, H.Y. Wu, P.F. Liang, Y.Y. Yang, Y.H. Lam, P. Ma, F.F. Duan, Z.H. Gao, Q. Hu, Z. Bai, J.B. Ma, J.G. Wang, F.P. Zhong, C.G. Wu, D.W. Luo, Y. Jiang, Y. Liu, D.S. Hou, R. Li, N.R. Ma, W.H. Ma, G.Z. Shi, G.M. Yu, D. Patel, S.Y. Jin, Y.F. Wang, Y.C. Yu, Q.W. Zhou, P. Wang, L.Y. Hu, X. Wang, H.L. Zang, P.J. Li, Q.Q. Zhao, L. Yang, P.W. Wen, F. Yang, H.M. Jia, G.L. Zhang, M. Pan, X.Y. Wang, H.H. Sun, Z.G. Hu, R.F. Chen, M.L. Liu, W.Q. Yang, Y.M. Zhao, H.Q. Zhang, Phys. Rev. C **99**, 064312 (2019). https://doi.org/10.1103/PhysRevC.99.064312
102. C. Hornung, D. Amanbayev, I. Dedes, G. Kripko-Koncz, I. Miskun, N. Shimizu, S. Ayet San Andrés, J. Bergmann, T. Dickel, J. Dudek, J. Ebert, H. Geissel, M. Górska, H. Grawe, F. Greiner, E. Haettner, T. Otsuka, W.R. Plaß, S. Purushothaman, A.K. Rink, C. Scheidenberger, H. Weick, S. Bagchi, A. Blazhev, O. Charviakova, D. Curien, A. Finlay, S. Kaur, W. Lippert, J.H. Otto, Z. Patyk, S. Pietri, Y.K. Tanaka, Y. Tsunoda, J.S. Winfield, Phys. Lett. B **802**, 135200 (2020). https://doi.org/10.1016/j.physletb.2020.135200
103. D. Puentes, Z. Meisel, G. Bollen, A. Hamaker, C. Langer, E. Leistenschneider, C. Nicoloff, W.J. Ong, M. Redshaw, R. Ringle, C.S. Sumithrarachchi, J. Surbrook, A.A. Valverde, I.T. Yandow, Phys. Rev. C **106**, L012801 (2022). https://doi.org/10.1103/PhysRevC.106.L012801
104. M. Chartier, W. Mittig, N.A. Orr, J.C. Angélique, G. Audi, J.M. Casandjian, A. Cunsolo, C. Donzaud, A. Foti, A. Lépine-Szily, M. Lewitowicz, S. Lukyanov, M. Mac Cormick, D.J. Morrissey, A.N. Ostrowski, B.M. Sherrill, C. Stephan, T. Suomijärvi, L. Tassan-Got, D.J. Vieira, A.C.C. Villari, J.M. Wouters, Nucl. Phys. A **637**, 3 (1998). https://doi.org/10.1016/S0375-9474(98)00228-0
105. Z. Meisel, S. George, Int. J. Mass Spectrom. **349–350**, 145 (2013). https://doi.org/10.1016/j.ijms.2013.03.022
106. Z. Meisel, S. George, S. Ahn, D. Bazin, B.A. Brown, J. Browne, J.F. Carpino, H. Chung, R.H. Cyburt, A. Estradé, M. Famiano, A. Gade, C. Langer, M. Matoš, W. Mittig, F. Montes, D.J. Morrissey, J. Pereira, H. Schatz, J. Schatz, M. Scott, D. Shapira, K. Smith, J. Stevens, W. Tan, O. Tarasov, S. Towers, K. Wimmer, J.R. Winkelbauer, J. Yurkon, R.G.T. Zegers, Phys. Rev. C **101**, 052801 (2020). https://doi.org/10.1103/PhysRevC.101.052801
107. S. Brett, I. Bentley, N. Paul, R. Surman, A. Aprahamian, Eur. Phys. J. A **48**, 184 (2012). https://doi.org/10.1140/epja/i2012-12184-4
108. A. Aprahamian, I. Bentley, M. Mumpower, R. Surman, AIP Adv. **4**, 041101 (2014). https://doi.org/10.1063/1.4867193
109. M. Mumpower, R. Surman, D.L. Fang, M. Beard, A. Aprahamian, J. Phys. G Nucl. Part. Phys. **42**, 034027 (2015). https://doi.org/10.1088/0954-3899/42/3/034027
110. M.R. Mumpower, R. Surman, D.L. Fang, M. Beard, P. Möller, T. Kawano, A. Aprahamian, Phys. Rev. C **92**, 035807 (2015). https://doi.org/10.1103/PhysRevC.92.035807
111. M. Mumpower, R. Surman, A. Aprahamian, EPJ Web Conf. **93**, 03003 (2015). https://doi.org/10.1051/epjconf/20159303003

112. T.M. Sprouse, R. Navarro Perez, R. Surman, M.R. Mumpower, G.C. McLaughlin, N. Schunck, Phys. Rev. C **101**, 055803 (2020). https://doi.org/10.1103/PhysRevC.101.055803
113. X.F. Jiang, X.H. Wu, P.W. Zhao, Astrophys. J. **915**, 29 (2021). https://doi.org/10.3847/1538-4357/ac042f
114. N. Vassh, G.C. McLaughlin, M.R. Mumpower, R. Surman, Astrophys. J. **907**, 98 (2021). https://doi.org/10.3847/1538-4357/abd035
115. N. Vassh, G.C. McLaughlin, M.R. Mumpower, R. Surman, Front. Phys. **10**, 1046638 (2022). https://doi.org/10.3389/fphy.2022.1046638
116. M. Mumpower, R. Surman, G. McLaughlin, A. Aprahamian, Prog. Part. Nucl. Phys. **86**, 86 (2016). https://doi.org/10.1016/j.ppnp.2015.09.001
117. H.F. Li, S. Naimi, T.M. Sprouse, M.R. Mumpower, Y. Abe, Y. Yamaguchi, D. Nagae, F. Suzaki, M. Wakasugi, H. Arakawa, W.B. Dou, D. Hamakawa, S. Hosoi, Y. Inada, D. Kajiki, T. Kobayashi, M. Sakaue, Y. Yokoda, T. Yamaguchi, R. Kagesawa, D. Kamioka, T. Moriguchi, M. Mukai, A. Ozawa, S. Ota, N. Kitamura, S. Masuoka, S. Michimasa, H. Baba, N. Fukuda, Y. Shimizu, H. Suzuki, H. Takeda, D.S. Ahn, M. Wang, C.Y. Fu, Q. Wang, S. Suzuki, Z. Ge, Y.A. Litvinov, G. Lorusso, P.M. Walker, Z. Podolyak, T. Uesaka, Phys. Rev. Lett. **128**, 152701 (2022). https://doi.org/10.1103/PhysRevLett.128.152701
118. M.R. Mumpower, G.C. McLaughlin, R. Surman, Phys. Rev. C **85**, 045801 (2012). https://doi.org/10.1103/PhysRevC.85.045801
119. M.R. Mumpower, G.C. McLaughlin, R. Surman, Astrophys. J. **752**, 117 (2012). https://doi.org/10.1088/0004-637X/752/2/117
120. M.R. Mumpower, G.C. McLaughlin, R. Surman, A.W. Steiner, Astrophys. J. **833**, 282 (2016). https://doi.org/10.3847/1538-4357/833/2/282
121. M.R. Mumpower, G.C. McLaughlin, R. Surman, A.W. Steiner, J. Phys. G Nucl. Part. Phys. **44**, 034003 (2017). https://doi.org/10.1088/1361-6471/44/3/034003
122. R. Orford, N. Vassh, J.A. Clark, G.C. McLaughlin, M.R. Mumpower, G. Savard, R. Surman, A. Aprahamian, F. Buchinger, M.T. Burkey, D.A. Gorelov, T.Y. Hirsh, J.W. Klimes, G.E. Morgan, A. Nystrom, K.S. Sharma, Phys. Rev. Lett. **120**, 262702 (2018). https://doi.org/10.1103/PhysRevLett.120.262702
123. M. Vilen, J.M. Kelly, A. Kankainen, M. Brodeur, A. Aprahamian, L. Canete, T. Eronen, A. Jokinen, T. Kuta, I.D. Moore, M.R. Mumpower, D.A. Nesterenko, H. Penttilä, I. Pohjalainen, W.S. Porter, S. Rinta-Antila, R. Surman, A. Voss, J. Äystö, Phys. Rev. Lett. **120**, 262701 (2018). https://doi.org/10.1103/PhysRevLett.120.262701
124. M. Vilen, J.M. Kelly, A. Kankainen, M. Brodeur, A. Aprahamian, L. Canete, R.P. de Groote, A. de Roubin, T. Eronen, A. Jokinen, I.D. Moore, M.R. Mumpower, D.A. Nesterenko, J. O'Brien, A.P. Perdomo, H. Penttilä, M. Reponen, S. Rinta-Antila, R. Surman, Phys. Rev. C **101**, 034312 (2020). https://doi.org/10.1103/PhysRevC.101.034312
125. R. Orford, N. Vassh, J.A. Clark, G.C. McLaughlin, M.R. Mumpower, D. Ray, G. Savard, R. Surman, F. Buchinger, D.P. Burdette, M.T. Burkey, D.A. Gorelov, J.W. Klimes, W.S. Porter, K.S. Sharma, A.A. Valverde, L. Varriano, X.L. Yan, Phys. Rev. C **105**, L052802 (2022). https://doi.org/10.1103/PhysRevC.105.L052802
126. N. Vassh, R. Vogt, R. Surman, J. Randrup, T.M. Sprouse, M.R. Mumpower, P. Jaffke, D. Shaw, E.M. Holmbeck, Y. Zhu, G.C. McLaughlin, J. Phys. G Nucl. Part. Phys. **46**, 065202 (2019). https://doi.org/10.1088/1361-6471/ab0bea
127. N. Vassh, M.R. Mumpower, G.C. McLaughlin, T.M. Sprouse, R. Surman, Astrophys. J. **896**, 28 (2020). https://doi.org/10.3847/1538-4357/ab91a9
128. N. Vassh, G.C. McLaughlin, M.R. Mumpower, R. Surman (2022). https://doi.org/10.48550/ARXIV.2202.09437
129. P. Möller, B. Pfeiffer, K.L. Kratz, Phys. Rev. C **67**, 055802 (2003). https://doi.org/10.1103/PhysRevC.67.055802
130. S.J. Fujimoto, M.A. Hashimoto, Mon. Not. R. Astron. Soc. Lett. **493**, L103 (2020). https://doi.org/10.1093/mnrasl/slaa016
131. G.W. Misch, S.K. Ghorui, P. Banerjee, Y. Sun, M.R. Mumpower, Astrophys. J. Suppl. Ser. **252**, 2 (2021). https://doi.org/10.3847/1538-4365/abc41d
132. G.W. Misch, T.M. Sprouse, M.R. Mumpower, Astrophys. J. Lett. **913**, L2 (2021). https://doi.org/10.3847/2041-8213/abfb74
133. G.W. Misch, T.M. Sprouse, M.R. Mumpower, A.J. Couture, C.L. Fryer, B.S. Meyer, Y. Sun, Symmetry **13**, 1831 (2021). https://doi.org/10.3390/sym13101831
134. L. Neufcourt, Y. Cao, W. Nazarewicz, F. Viens, Phys. Rev. C **98**, 034318 (2018). https://doi.org/10.1103/PhysRevC.98.034318
135. L. Neufcourt, Y. Cao, S.A. Giuliani, W. Nazarewicz, E. Olsen, O.B. Tarasov, Phys. Rev. C **101**, 044307 (2020). https://doi.org/10.1103/PhysRevC.101.044307
136. A.E. Lovell, A.T. Mohan, T.M. Sprouse, M.R. Mumpower, Phys. Rev. C **106**, 014305 (2022). https://doi.org/10.1103/PhysRevC.106.014305
137. M.R. Mumpower, T.M. Sprouse, A.E. Lovell, A.T. Mohan, Phys. Rev. C **106**, L021301 (2022). https://doi.org/10.1103/PhysRevC.106.L021301

Springer Nature or its licensor (e.g. a society or other partner) holds exclusive rights to this article under a publishing agreement with the author(s) or other rightsholder(s); author self-archiving of the accepted manuscript version of this article is solely governed by the terms of such publishing agreement and applicable law.